Towards magnetic control of magnetite

F.J. Pedrosa, J.L.F. Cuñado, P. Perna, M. Sanz, M. Oujja, E. Rebollar, J.F. Marco, J. de la Figuera, M. Monti, M. Castillejo, M. Garcia-Hernández, F. Mompeán, J. Camarero, A. Bollero

Towards magnetic control of magnetite

F. J. Pedrosa,[1] J.L.F. Cuñado,[1,4] P. Perna,[1] M. Sanz,[2] M. Oujja,[2] E. Rebollar,[2] J.F. Marco,[2] J. de la Figuera,[2] M. Monti,[2] M. Castillejo,[2] M. García-Hernández,[3] F. Mompeán,[3] J. Camarero,[1,4] and A. Bollero[1]

[1] Instituto Madrileño de Estudios Avanzados en Nanociencia, IMDEA Nanociencia, Campus Universidad Autónoma de Madrid, 28049, Madrid, Spain

[2] Instituto de Química Física "Rocasolano", IQFR-CSIC, 28006, Madrid, Spain

[3] Instituto de Ciencia de Materiales, ICMM-CSIC, Campus Universidad Autónoma de Madrid, 28049 Madrid, Spain

[4] Departamento de Física de la Materia Condensada and Instituto "Nicolás Cabrera", Universidad Autónoma de Madrid, Campus Universidad Autónoma de Madrid, 28049 Madrid, Spain

E-mail: `javier.pedrosa@imdea.org`

E-mail: `alberto.bollero@imdea.org`

14 May 2019

Abstract.

High quality stoichiometric magnetite (Fe_3O_4) films grown by infrared pulsed laser deposition (IR-PLD) on different surfaces have been investigated in order to study the influence of the substrate, orientation, and thickness on their magnetic behavior. Different single crystal (001)-oriented substrates, i.e., $SrTiO_3$(001), $MgAl_2O_4$(001)and MgO(001), have been used for the preparation of epitaxial Fe_3O_4(001) films. By comparison, polycrystalline magnetite films were obtained on both single crystal Al_2O_3(0001) and amorphous Si/SiO_2 substrates. The thickness has been varied between 50 - 400 nm. All films consist of nanocrystalline stoichiometric magnetite with very small strain ($< 1\%$) and present the Verwey transition (T_V) between 110-120 K, i.e., close to bulk magnetite (122 K). In general, T_V depends on both microstructure and thickness, increasing mainly as the thickness increases. Room temperature angular-dependent measurements reveal an in-plane fourfold symmetry magnetic behavior for all films grown on (001)-oriented surfaces, and with the easy axes lying along the Fe_3O_4[010] and [100] directions. Remarkably, the fourfold magnetic symmetry shows up to 400 nm thick films. In turn, the films grown on single crystal Al_2O_3(0001) and on amorphous Si/SiO_2 surfaces display an isotropic magnetic behavior. In general, the coercive field (H_C) depends on microstructure and film thickness. The largest (lowest) H_C value has been found for the thinner film grown on a single crystal $SrTiO_3$(001) (amorphous Si/SiO_2) surface, which present the largest (lowest) strain (crystallinity). Moreover, the coercivity follows an inverse law with film thickness. Our results demonstrate that we can artificially control the magnetic behavior of stoichiometric IR-PLD grown Fe_3O_4 films by exploiting substrate-induced anisotropy and thickness-controlled coercivity, that might be relevant to incorporate magnetite in future spintronic devices.

1. Introduction

Magnetite (Fe_3O_4) is a ubiquitous iron oxide mineral that is the most magnetic of all the naturally-occurring minerals on Earth [1]. In the last decades, artificially grown magnetite films have shown great potential for spintronic applications [2–4], due to its robust ferrimagnetism down to nanometer thickness, high Curie temperature (858 K), good electrical conductivity and presumed half-metal character [1, 5], which require well-defined and controlled magnetic behavior. Fe_3O_4 presents an inverse spinel crystalline structure at room temperature (Fig. 1.a), with a third of Fe atoms (Fe^{3+}) occupying the tetrahedral A-sites and the rest (Fe^{2+} and Fe^{3+}) on the octahedral B-sites. It presents a low-temperature metal-insulator transition known as the Verwey transition (T_V) [6, 7], whose temperature and character depends on crystal quality [8, 9], where the crystalline structure changes from cubic to monoclinic. Different routes have been used to prepare magnetite thin films, such as molecular beam epitaxy (MBE) [9–15], sputtering [16–19] and pulsed laser deposition (PLD) [20–24], and also on different substrates such as MgO, Al_2O_3, $MgAl_2O_4$, $BaTiO_3$ and $SrTiO_3$. However, there is at present no general consensus regarding the magnetic behavior of magnetite films. An open question is to what extent the preparation of Fe_3O_4 films can affect their detailed magnetic properties, including remanence, coercive field, and magnetic anisotropy symmetry.

In general, device applications based on magnetic nanostructures require both understanding and control of the magnetic behavior of artificially grown films, where the magnetic properties can differ from the bulk ones and, in addition, can be influenced by the film growth microstructure, including interfacial strain, crystal orientation and thickness. The magnetization bulk easy-axis directions of Fe_3O_4 at room temperature (RT) are the cubic $\langle 111 \rangle$ ones (dashed red vectors in Fig. 1.b). Thus, in the (001) surface of bulk samples, the magnetization is expected to lie along the in-plane $\langle 110 \rangle$ directions (blue vectors in Fig. 1.b), i.e., the projection of the bulk $\langle 111 \rangle$ on the (001) surface, as confirmed by magnetic microscopy observations [25]. In the case of artificially grown magnetite films, many works have focused on the study of in-plane magnetic anisotropy induced by the substrate [11, 18, 23, 26–33, 54]. The MgO substrates have been widely explored [11, 12, 26–31] due to its low lattice mismatch with Fe_3O_4 (+0.3%). In general, in-plane magnetic anisotropies have been reported for magnetite grown on MgO(001) and MgO(110) substrates [11, 26–31]. However, in-plane isotropic behavior has been also reported [30]. Recently, some works reported perpendicular magnetic anisotropy in Fe_3O_4 films deposited on MgO(111) substrates [28]. Other oxide (001)-oriented substrates with larger lattice mismatch have been used, such as $MgAl_2O_4$ (misfit −3.9%) [24], $SrTiO_3$ (misfit −7.0%) [17, 29–31], and $LaAlO_3$ (misfit −9.7%) [17], resulting in a well-defined magnetic anisotropy of very small strained Fe_3O_4 films ($< 1\%$) with thicknesses above 40 nm. In addition, semiconductor single crystals substrates such as GaAs(001) [33], InAs(001) [34], and buffered Si(001) [19, 32], as well as metallic substrates [54], have been also used to induce in-plane anisotropy.

However, there is no consensus about the easy axis direction in the films showing

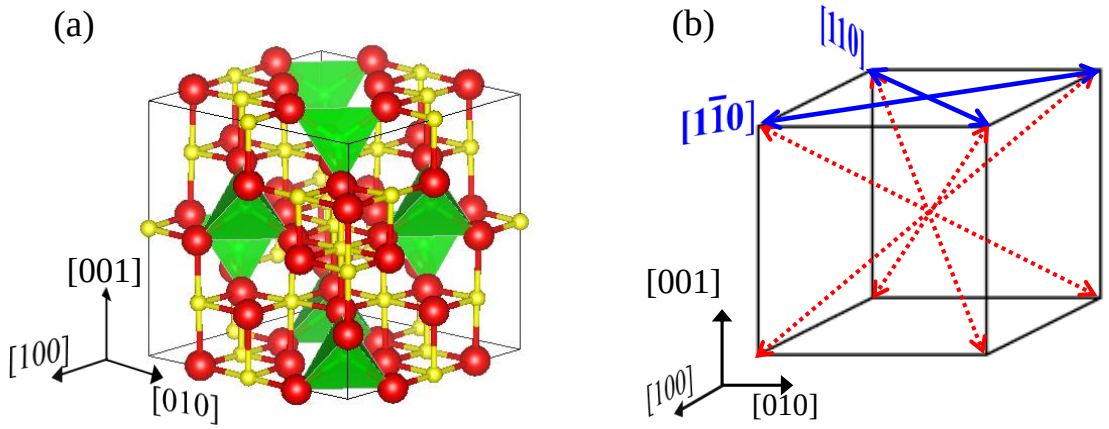

Figure 1. Schematic illustration showing the crystal unit cell (a) and the magnetic symmetry of Fe_3O_4(001) single crystal at room temperature. The crystal scheme has been prepared by VESTA [40], with tetrahedral and octahedral sites of the inverse spinel structure indicated in (a). The eight anisotropy directions of bulk magnetite, i.e., ⟨111⟩ crystal directions, are indicated with dashed red vectors in (b), which results with a fourfold in-plane magnetic symmetry in the surface plane with easy axis directions along the ⟨110⟩ surface crystal directions, indicated with blue vectors.

what in-plane anisotropic behavior is. In most cases, the ⟨110⟩ surface in-plane directions are reported for the easy-axis, as expected from a (001)-oriented surface of bulk magnetite (see Fig. 1.b), but they do not identify the local domain magnetization direction. Recently, we showed ⟨100⟩ magnetization easy axes in magnetite films grown on $SrTiO_3$:Nb(100) [23]. The main result of this work is shown in Fig. 2. In particular, stoichiometric epitaxial Fe_3O_4 thin films grown with PLD on $SrTiO_3$:Nb(001) substrates (Fig. 2.A) showed individual domains with magnetization lying mostly along the in-plane ⟨100⟩ directions (Fig. 2.B), while the domain walls were aligned with the ⟨110⟩ directions. Furthermore, the remanence and the coercivity display an in-plane fourfold symmetry with the maxima of both along the ⟨100⟩ directions (Fig. 2.C). Similar results have been reported in magnetite films grown by sputtering [17, 19] and PLD [20, 24] on different substrates, in which hysteresis loops acquired along different directions are compared.

Other important magnetic parameters of magnetite films like the magnetization reversal mechanism and the coercivity are much less investigated. The magnetization reversal understanding requires either magnetic imaging and/or a vectorial-analysis of the magnetization reversal. In turn, the coercivity is not a direct measure of the strength of anisotropy. It is modified by defects and may present strong dynamical effects [35], but its angular dependence can provide information on the dynamic effective magnetic anisotropy symmetry, and its evolution with thickness can indicate general trends, if any. Apart of the angular dependence measurements for specific thicknesses and substrates mentioned below, we are not aware of the aforementioned studies that are required, nor general trends have been identified yet.

From the above discussion, it is well established that the properties of magnetite films are determined by the film microstructure, including interfacial strain, crystal orientation and thickness. Thus, both magnetic and transport properties are strongly influenced by the synthesis method and growth conditions. For instance, poor quality films present the Verwey transition at a lower temperature [8, 9]. Moreover, several results indicate that the magnetism and magneto-transport phenomena in magnetite films are controlled by antiphase domain boundaries (APBs) generated during the film growth [13, 36]. In fact, the crystal domain size or the APB density seems to be dependent on the thickness [31, 37] and on the misfit with the substrate [30]. Therefore, it is clear that precise control over the microstructure and phase purity is necessary to control the magnetic behavior, and therefore the transport behavior. Furthermore, in order to disentangle the magnetic symmetry orientation and to study its dependence

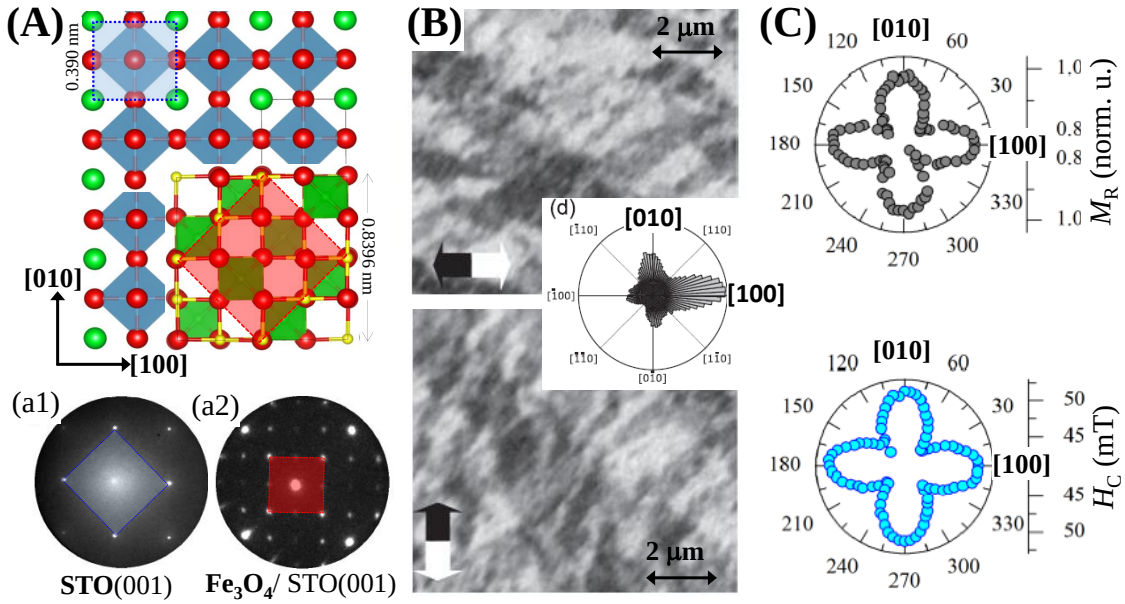

Figure 2. Identifying magnetic easy-axis directions of stoichiometric magnetite films grown on $SrTiO_3$:Nb(001) [23]. (A) Epitaxial relationship of magnetite on $SrTiO_3$. Oxygen atoms are shown as red spheres, with Sr atoms represented by green ones (Ti atoms are below in the middle of the blue-grey octahedral). The magnetite unit cell is shown in the lower-right side, with octahedral irons shown in yellow, and tetrahedral irons shown as green filled tetrahedra (schematics prepared by VESTA [40]). The surface unit cells of both materials are drawn by blue and red squares, respectively (a1) and (a2) Corresponding LEED patterns measured by LEEM (both images are at the same scale). (B) Room temperature SPLEEM images acquired at the same location with the electron spin-direction along the x-axis ([100] direction, top image) and y-axis ($[0\bar{1}0]$, bottom), showing the local surface magnetization component along the given direction. The inset shows the corresponding polar histogram of the in-plane magnetization as derived from the images. (C) Polar plot representation of the remanence (top graph) and coercivity (bottom) derived from kerr hysteresis loops acquired at different applied field angles with respect to the [100] crystal direction (Adapted from [23]).

with the aforementioned microstructure parameters, a study of the angular evolution of the magnetic properties is required.

In this work, we study pure magnetite films grown by IR-PLD upon changing substrate, orientation, and thickness. The morphology, microstructure, stoichiometry, Verwey transition, and angular-dependent magnetic behavior of all films prepared have been correlated in order to identify the key parameters controlling the magnetic properties of high quality nanostructured magnetite films grown by IR-PLD.

2. Experimental

High quality magnetite films grown on different substrates, and with different thicknesses, have been investigated in detail in order to get the key parameters controlling the magnetic behavior. Pulsed laser deposition (PLD) has been used for the deposition [38]. Both laser irradiation wavelength and substrate temperature crucially affect the composition, crystallinity, surface structure and the magnetic properties of the grown samples. PLD investigations of magnetite thin films are routinely performed with ultraviolet (UV)[39] lasers. However we have recently demonstrated the preparation of high quality magnetite films by using 1064 nm infrared-wavelength irradiation (IR-PLD) [22] from hematite targets.

For the present study, magnetite films of different thickness, ranging from 30 to 450 nm, have been prepared on different surfaces, including substrates with cubic, hexagonal, and amorphous structure. In order to study the possible influence of the substrate lattice parameter on microstructure and magnetic properties of the magnetite films (bulk lattice parameter of 0.8395 nm), we have chosen different (001)-oriented substrates with different lattice mismatch with magnetite: MgO (mismatch with magnetite is -0.3 %, tensile), $MgAl_2O_4$ (MAO, +3.9 %, compressive), $SrTiO_3$ (STO, +7.3 %, compressive), and $SrTiO_3$:Nb (STO:Nb, +7.3 %, compressive). As examples of non-cubic substrates we have used amorphous substrate Si/SiO_x and hexagonal $Al_2O_3(0001)$ substrates.

The Q-switched Nd:YAG laser had a full width at half-maximum of 15 ns with a 10 Hz repetition rate at a typical fluence of 4 J/cm^2. The substrates were heated to 750 K during deposition. Layer thicknesses were determined ex situ either by X-Ray fluorescence and/or by X-ray reflectometry. The morphology, microstructure, and stoichiometry of the films were characterized at room temperature (RT) by atomic force microscopy (AFM), X-Ray diffraction (XRD) and Mössbauer spectroscopy, respectively. Mössbauer data were recorded in the electron detection mode using a conventional constant acceleration spectrometer equipped with a ^{57}Co(Rh) source and a parallel plate avalanche counter [41]. The velocity scale was calibrated using an α-iron foil and the isomer shifts were referred to the centroid of the centroid of the RT spectrum of α-iron.

Magnetic characterization was carried out by superconducting quantum interference device magnetometry (SQUID) and vectorial-resolved magneto-optical Kerr effect (v-

MOKE). SQUID magnetometry is employed to measure the evolution of magnetization with temperature, which has been used to determine the Verwey transition of the investigated magnetite thin films. The angular dependence of the Fe_3O_4 films magnetic properties was measured at room temperature (RT) by high-resolution v-MOKE measurements in a longitudinal configuration [42, 43]. The hysteresis loops were recorded by changing the in-plane angular rotation of the sample (α_H) and keeping fixed the external magnetic field direction, which is applied parallel to the film plane. The whole angular range was probed at intervals of 4.5°, i.e., from $\alpha_H = 0°$ to 360°.

3. Results

In the following, relevant results on the morphology, chemical, and structural characterization of the different films investigated will be presented. Representative microscopy AFM images of the magnetite films grown on different substrates are shown

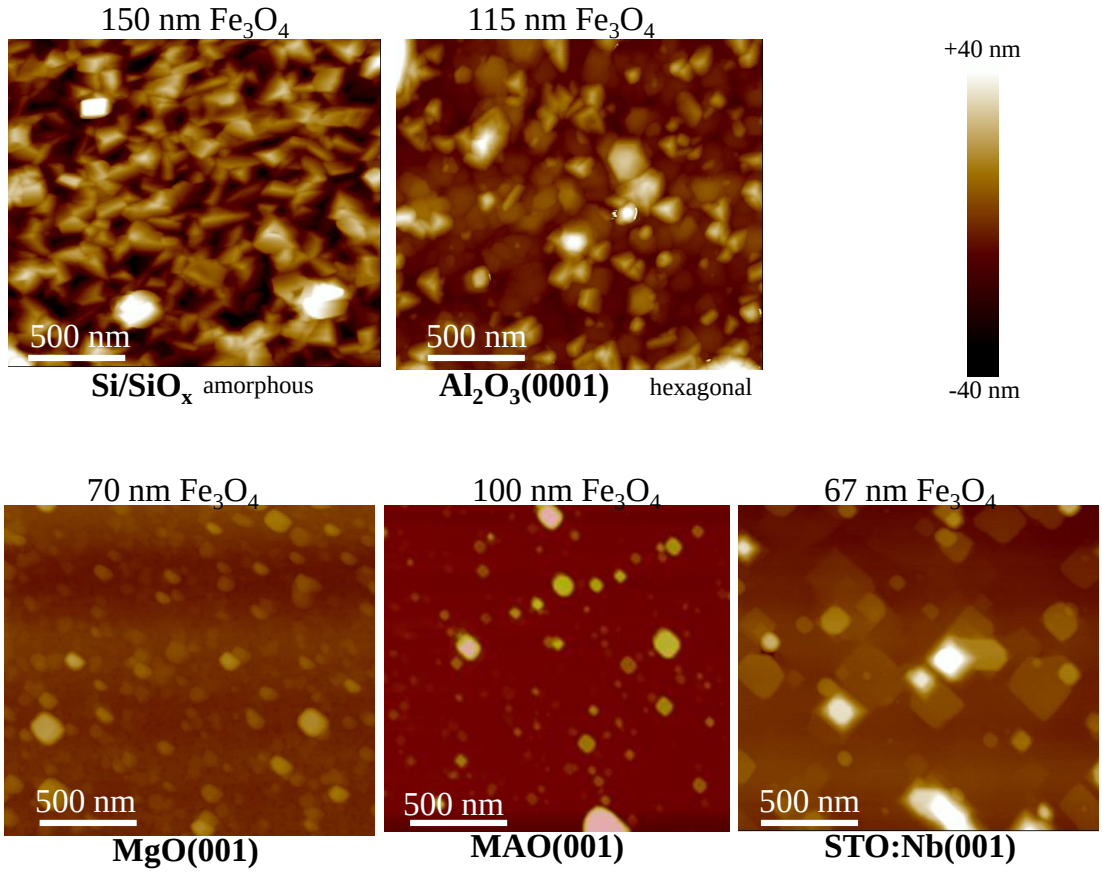

Figure 3. Surface topography characterization. Selected AFM topographic images, 2.0μm wide of Fe_3O_4 thin films grown on non-cubic (top images: amorphous SiO_2 and hexagonal $Al_2O_3(0001)$) and cubic (bottom: $MgO(001)$, $MgAl_2O_3(001)$ and $SrTiO_3(001)$) substrates. The thermal color height scale is displayed in the right top side and corresponds to 40 nm.

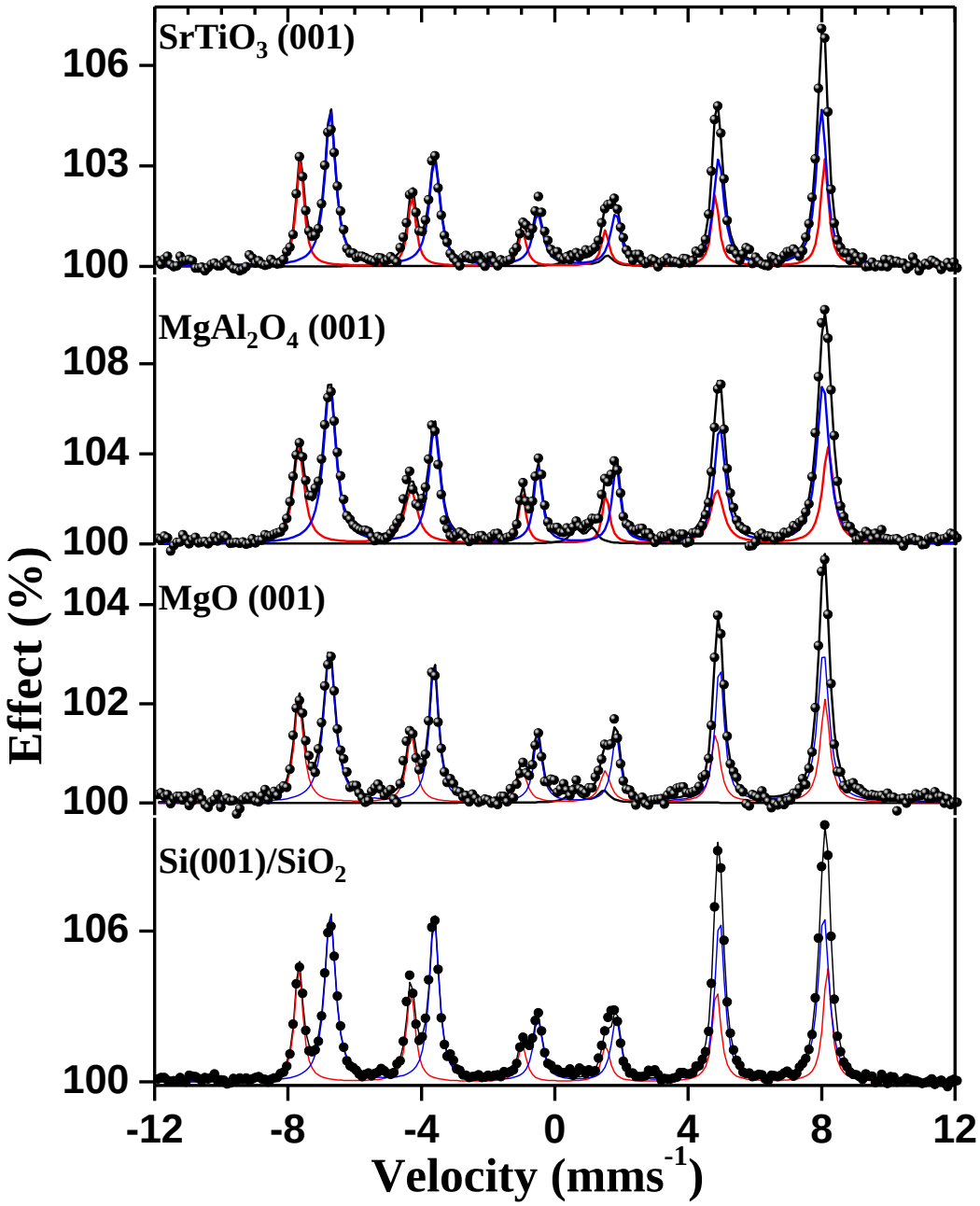

Figure 4. Room temperature ICEMS spectra recorded from the Fe_3O_4 films grown on the indicated surfaces. The symbols are the experimental data acquired in the films used in Fig. 3. Continuous black lines are the best fits with the two sextet components, as expected for magnetite. The corresponding resonances S_A and S_B are depicted with solid red and blue lines, respectively. Note that the ratios S_B/S_A found indicate that the films have stoichiometric composition while the area ratio of the lines 2 and 3 of sextets indicate the existence of out-of-plane magnetization components.

in Fig. 3. In general, the root-mean-square roughness (roughness in the following) is much larger in the case of non-cubic substrates (> 20 nm), where pronounced elongated, squared, and orthorhombic features for films hundred nanometer thick with sharp edges can be identified (first two left images of Fig.3). Smaller features are found in the film grown on the Al_2O_3(0001) surface. For the films deposited on (100)-oriented substrates, squared shape features ("mesas"), with heights of up to 30 nm and lateral sizes in the 100-200 nm range, emerge from a very flat film (with roughness < 3 nm), similar to our previous results on STO:Nb [23]. Moreover, the roughness increases with the lattice mismatch and with the thickness, suggesting that the lattice mismatch at the interface between both lattices is the main factor controlling the final morphology.

The good stoichiometry of the films has been checked by integral conversion electron Mössbauer spectroscopy (ICEMS) measurements at RT. The ICEMS spectrum of stoichiometric magnetite is composed by two sextets corresponding to the iron ions located in the octahedral (S_B) and tetrahedral (S_A) positions, respectively, of the spinel-related structure [44]. The ICEMS spectra recorded from various representative PLD films are depicted in Fig. 4 and all show these two sextets. For the sake of consistency all the spectra were fitted with the same criteria, basically maintaining the linewidth to be equal for the six line of sextets (but different for the S_A and S_B components) and the areas in the ratio 3:x:1:1:x:3, allowing x to refine until obtaining the best χ^2 value. In general, the Mössbauer parameters obtained from the fit of the spectra are totally characteristic of magnetite with x values around 2, between 1.8 (MgAl2O4) and 2.6 (Si) (being 2.2 for both MgO and STO). The latter is indicative that the films have out-of-plane magnetization components, where $x = 4$ corresponds to full in-plane magnetization and $x = 0$ to full out-of plane magnetization [58]. The derived Mössbauer parameters are: isomer shifts ($\delta A = 0.26$ mms^{-1} and $\delta B = 0.65$ mms^{-1}) quadrupole shifts ($2\epsilon_A = -0.02$ mms^{-1} and $2\epsilon_B = -0.02$ mms^{-1}) and hyperfine magnetic fields ($H_A = 49.0$ T and $H_B = 46.4$ T). The area ratio S_B/S_A of the two components is 1.9 in all the cases, what indicates that the films are of stoichiometric composition [44]. Thus, our data suggest that the substrate has no influence on the chemical composition of the films. The different x values found could be ascribed to the use of different substrates and thicknesses, as discussed in the next sections.

3.1. Influence of the substrate

The structural and magnetic characterization of magnetite films with similar thickness grown on different substrates are correlated and compared, in order to study the effect of the film's microstructure on its magnetic properties.

Figure 5 shows representative XRD patterns of Fe_3O_4 films grown on non-cubic substrates (a and b) and on (001)-oriented cubic substrates (c and d). The films grown on non-cubic substrates, i.e., on amorphous SiO_2 and Al_2O_3(0001), display peaks located at 30.2°, 35.5°, 37.1°, 57.2° and 62.7°, which are assigned to Fe_3O_4 reflections (220), (311), (220), (422), (511) and (440) planes, respectively (Fig. 5.a and

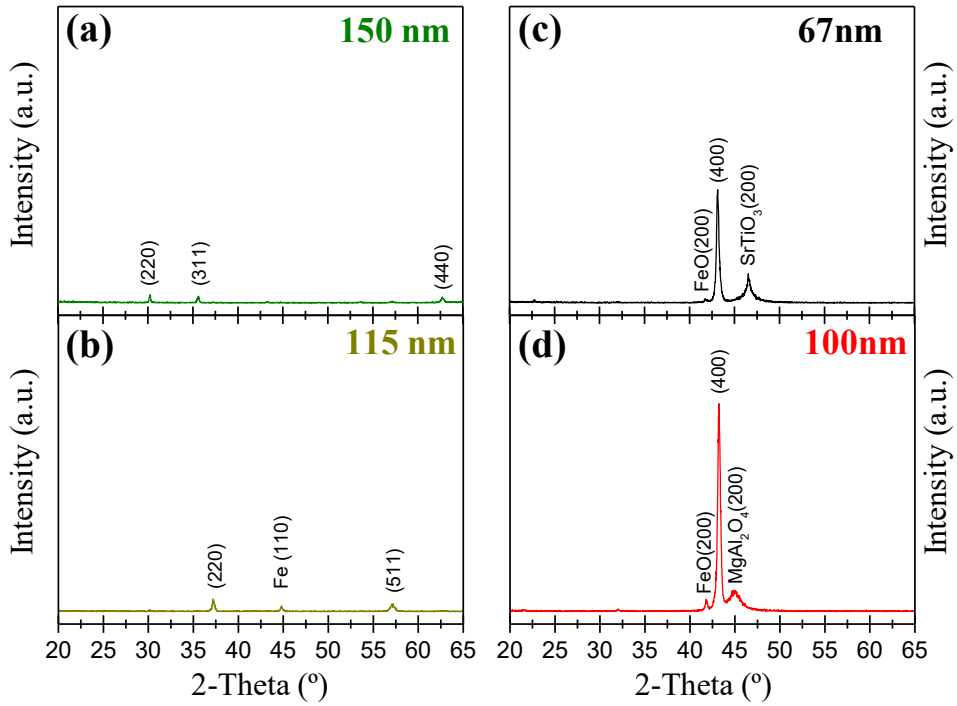

Figure 5. Selected XRD patterns of Fe_3O_4 thin films deposited on (a) Si(001) with a native SiO_2 layer, (b) Al_2O_3(0001), (c) $SrTiO_3$:Nb(001) and (d) $MgAl_2O_4$(001).

.b). This pattern is indicative of polycrystalline magnetite (Joint Committee on Powder Diffraction Standards Card No. 88-0866). An additional peak at 44.67° is observed on the film grown on Al_2O_3 substrate (Fig. 5.b). This peak is assigned to metallic iron. In contrast, the films grown on (001)-oriented cubic substrates ($SrTiO_3$:Nb and $MgAl_2O_4$) show a well-defined preferential orientation related to the surface of the substrate, as can be observed by the predominance of (400) reflection peak at an angle 43.3° (Fig. 5c and 5d). In this case, the films exhibit a small contribution of Wüstite ($Fe_{0.8}O_{0.2}$) that can be observed at an angle 41.8°. By comparing the intensity of peaks obtained for both families of substrates it can be noticed the high quality (crystallinity) of Fe_3O_4 films obtained when a (001)-oriented cubic substrate was employed.

Several structural parameters have been derived from the XRD patterns of Fig. 5. The average crystallite size have been calculated for all samples using Scherrer formula, resulting the following sizes: 28, 23, 31 and 50 nm for the Fe_3O_4 films grown on $SrTiO_3$:Nb, $MgAl_2O_4$, Al_2O_3 and SiO_2 substrates, respectively. The polycrystalline films have larger crystallite sizes when compared with the epitaxial ones of similar thickness. Moreover, larger crystallite sizes are found for the case of STO when compared with the other (001)-oriented cubic substrates. XRD patterns have been used as well to calculate the lattice parameter of the magnetite films, based on Bragg's law, obtaining values of 0.836, 0.836, 0.836 and 0.833 nm for SiO_2, Al_2O_3, $MgAl_2O_4$ and $SrTiO_3$:Nb substrates, respectively. Notice that all these values are quite close to the bulk one(0.840 nm), but with a small compressive strain ($< 1\%$).

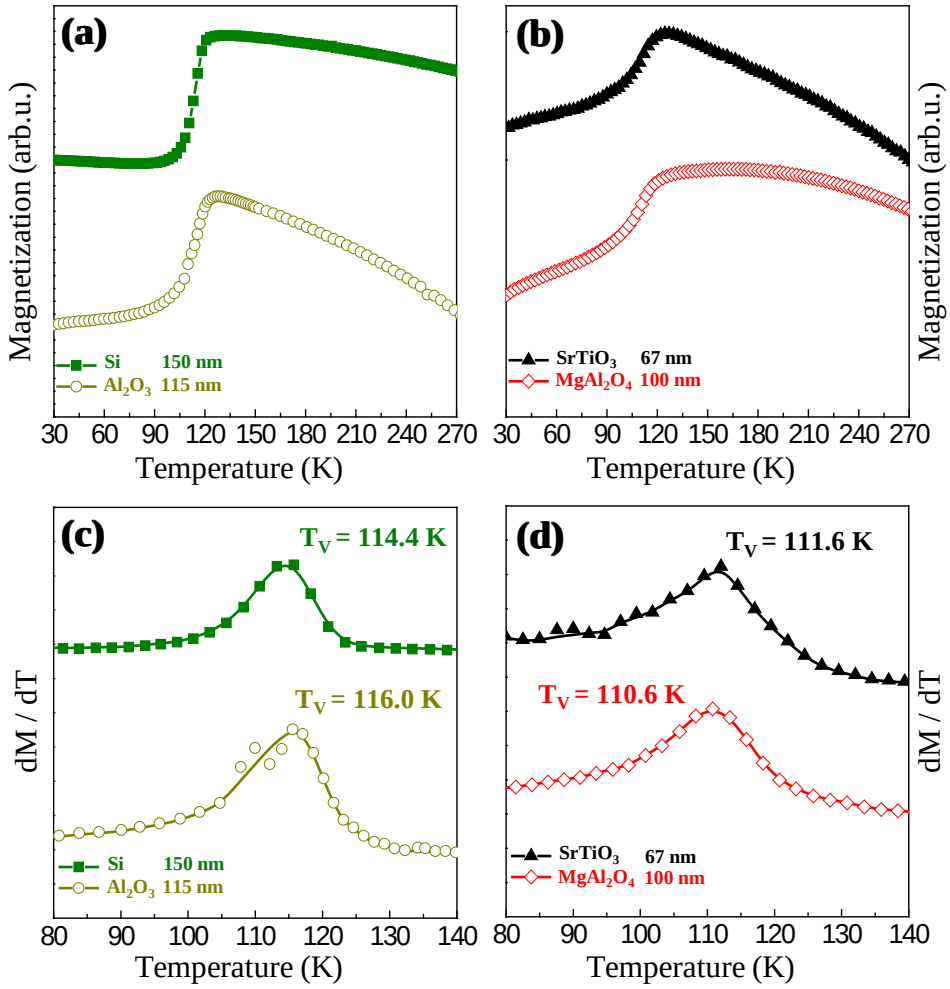

Figure 6. Determination of the Verwey transition temperature $T_{\rm v}$ for the polycrystalline (left graphs) and epitaxial (right) Fe_3O_4 films used in Fig. 5. In the top graphs the evolution of the films magnetization during the warming with an in-plane applied field of 2 kOe is plotted. On the bottom graphs, the corresponding temperature evolution of $\mathrm{d}M/\mathrm{d}T$ is plotted. For clarity, different colors and shapes have been used for the different Fe_3O_4 films: Si/SiO_2 with green square symbols, Al_2O_3 with dark yellow circles, $SrTiO_3$:Nb with black triangles; and $MgAl_2O_4$ with red diamonds, respectively. $T_{\rm v}$ is derived from the maximum value of the $\mathrm{d}M/\mathrm{d}T(T)$ curve.

The Verwey transition, which as mentioned depends strongly on crystal quality, was investigated by measuring the magnetization as a function of temperature. The transition is defined as the point with maximum rate of change in magnetization against temperature. A representative study for magnetite films of similar thickness grown on different substrates is displayed in Fig. 6. The evolution of the magnetization during warming of non-cubic and cubic substrates is compared in Fig. 6.a and Fig. 6.b, respectively. In order to identify clearly T_v, the evolution in temperature of the derivative of the magnetization with respect to the temperature has been plotted in Fig. 6.c and

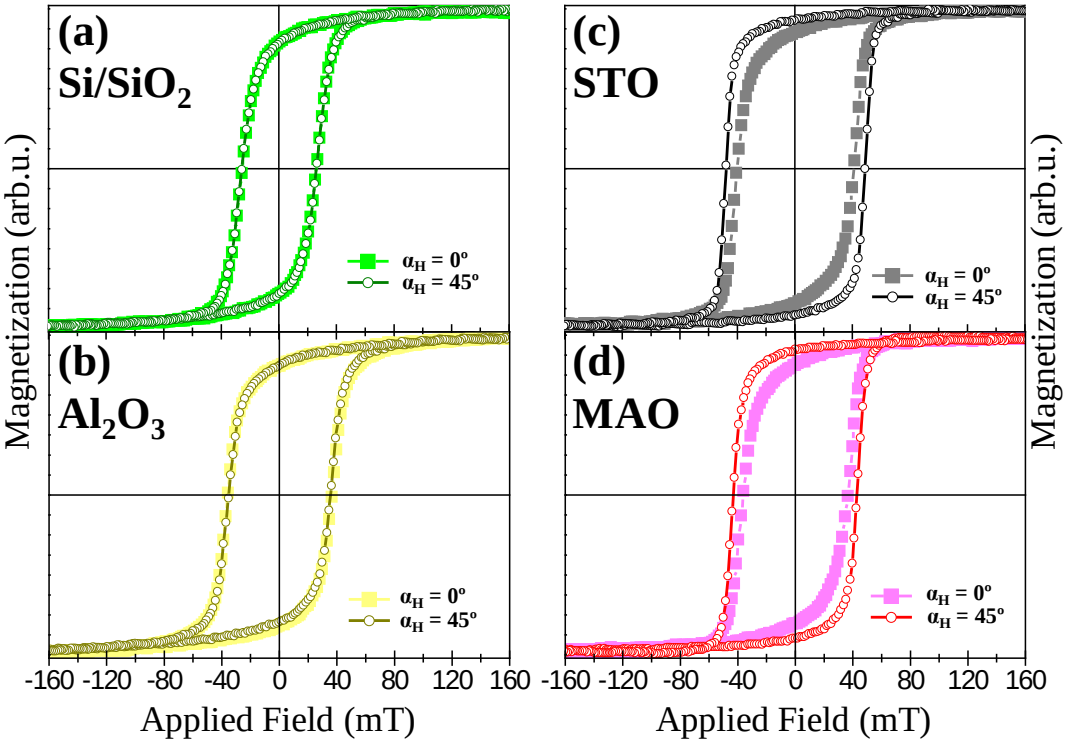

Figure 7. Selected in-plane hysteresis loops of Fe_3O_4 thin films deposited on (a) Si with a native SiO_2 layer, (b) Al_2O_3, (c) $SrTiO_3$:Nb and (d) $MgAl_2O_4$. Graphs (c) and (d) show hysteresis loops acquired at $\alpha_H = 0°$ and $\alpha_H = 45°$, which correspond to the easy and hard axis directions, respectively.

Fig. 6.d, respectively. T_v values of 114 and 116 K are obtained for the films grown on SiO_2 and Al_2O_3, respectively, while for $SrTiO_3$:Nb and $MgAl_2O_4$ the transition is found at 111 and 112 K, respectively. The difference of temperatures for the Verwey transition in different films might be related to strain induced by the substrate during first stages of growth, as well as to the crystalline average size [45]. For instance, polycrystalline films (with large crystallite size) have Verwey transition temperatures very close to the bulk magnetite value (120 K). By comparison, epitaxial Fe_3O_4 films (smaller crystallite size) present lower values. The difference also could be related with the thickness of the different films, because the epitaxial films are thinner than polycrystalline ones. In fact, T_V increases with increased thickness, as can be seen in Fig. 11.

Very clear differences can be observed when the magnetic properties of polycrystalline and epitaxial films are compared. MOKE hysteresis loops have been systematically recorded by changing the in-plane orientation of the applied magnetic field (α_H) in the whole angular range. Fig. 7 shows representative in-plane hysteresis loops measured at RT for Fe_3O_4 films deposited on different substrates. Two loops are plotted for each sample, with the applied magnetic field aligned along the [100] ($\alpha_H = 0°$) and [110] ($\alpha_H = 45°$) magnetite surface directions. Both hysteresis loops are identical for the case of polycrystalline films, i.e., films grown on SiO_2 and Al_2O_3

substrates, indicating an isotropic magnetic behavior (see Fig. 7.a and b). In contrast, a different magnetic behavior is identified for the two angular conditions in the case of films grown on $SrTiO_3$:Nb and $MgAl_2O_4$ substrates (Fig. 7.c and d). In this case, the hysteresis loops acquired at the two angular conditions show a different magnetization reversal pathway, and therefore different coercivity (H_C) and remanence (M_R) values. In particular, the remanence and coercivity values are higher for $\alpha_H = 0°$, i.e., along the [100] direction. The lowest coercivity and remanence values are found at $\alpha_H = 45°$, i.e., along the [110] direction. Between these, from $\alpha_H = 0°$ to 45°, both coercivity and remanence decrease and the opposite trend is found from $\alpha_H = 45°$ to 90°. In fact, the trend is repeated every 90° for the case of the epitaxial films, as shown in the corresponding polar-plots representations of coercivity and remanence depicted in Fig. 8. These clearly show a fourfold magnetic symmetry with the maxima along the $\langle 100 \rangle$ directions. By contrast, the polar-plots for films grown on SiO_2 and Al_2O_3 display no angular dependence of coercivity and remanence, indicative of an isotropic magnetic behavior of the polycrystalline films. This isotropic behaviour is also reflected (for out-of-plane vs in-plane) in the components of the Mössbauer spectra.

The fourfold symmetry is found for all epitaxial magnetite films grown on (001)-oriented oxide substrates and oriented along the $\langle 100 \rangle$ directions, i.e., rotated 45° with respect to the expected $\langle 110 \rangle$ surface directions (see Fig. 1). The difference between

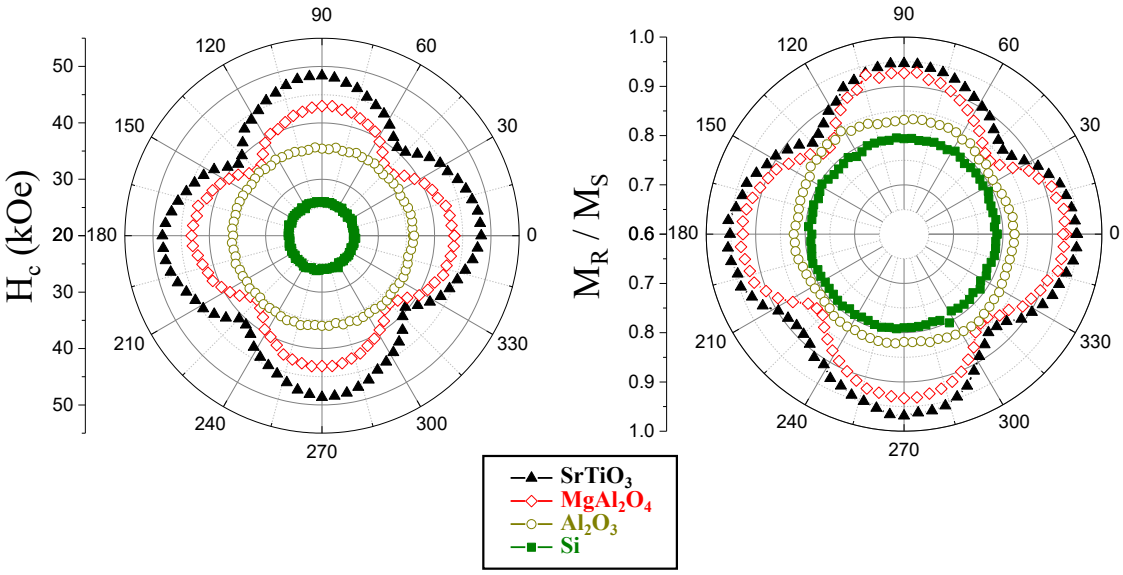

Figure 8. Polar-plot representations of the angular evolution of H_C and M_R/M_S of Fe_3O_4 thin films deposited on $SrTiO_3$:Nb (full triangles, black), $MgAl_2O_4$ (open diamonds, red), Al_2O_3 (open circles, dark yellow) and Si with a native SiO_2 layer (full squares, green). The symbols are derived from the corresponding hysteresis loops, as the one shown in Fig. 7, acquired at the different angular conditions in the whole range. Note the isotropic behavior of the polycrystalline magnetite films and the well-defined fourfold magnetic symmetry aligned along the $\langle 100 \rangle$ surface directions in the case of the epitaxial films.

Fe_3O_4 films grown on different substrates is the value of coercivity. For data shown in Fig. 8, the highest (smallest) coercivity values are found for the film grown on STO (Si). The difference in coercivity could be also attributed to the thickness difference of the films: the thinnest (thicker) film is the one grown on STO (Si). In the next section it is shown that, in fact, coercivity depends strongly on the films thickness.

3.2. Influence of film thickness

Figure 9 displays the diffraction patterns of Fe_3O_4(001) films of different thickness grown on STO:Nb and MAO. The increase of the Fe_3O_4 (400) peak intensity is clearly related with the increased thickness. Note that even for thicknesses as large as 330 and 350 nm, the films display a single crystal orientation, indicating the suitability of the IR-PLD technique to obtain thick Fe_3O_4(001) films with high crystallinity. The calculated strain of the films is similar when comparing the thin and the thick films grown on the same substrate. The one corresponding to STO:Nb is a little less relaxed; the strain on STO:Nb (MAO) is c.a. 0.8% (0.3%). The corresponding crystallite sizes, calculated using the Scherrer equation, are larger for the thicker films. The crystallite sizes are 28 and 70 nm (27 and 50 nm) for the films grown on STO:Nb (MAO) with thickness of 67 and 330 nm (100 and 350 nm).

The purity, i.e., good stoichiometry, of the magnetite films have been checked by ICEMS and by the determination of the Verwey transition T_V. In brief, the ICEMS

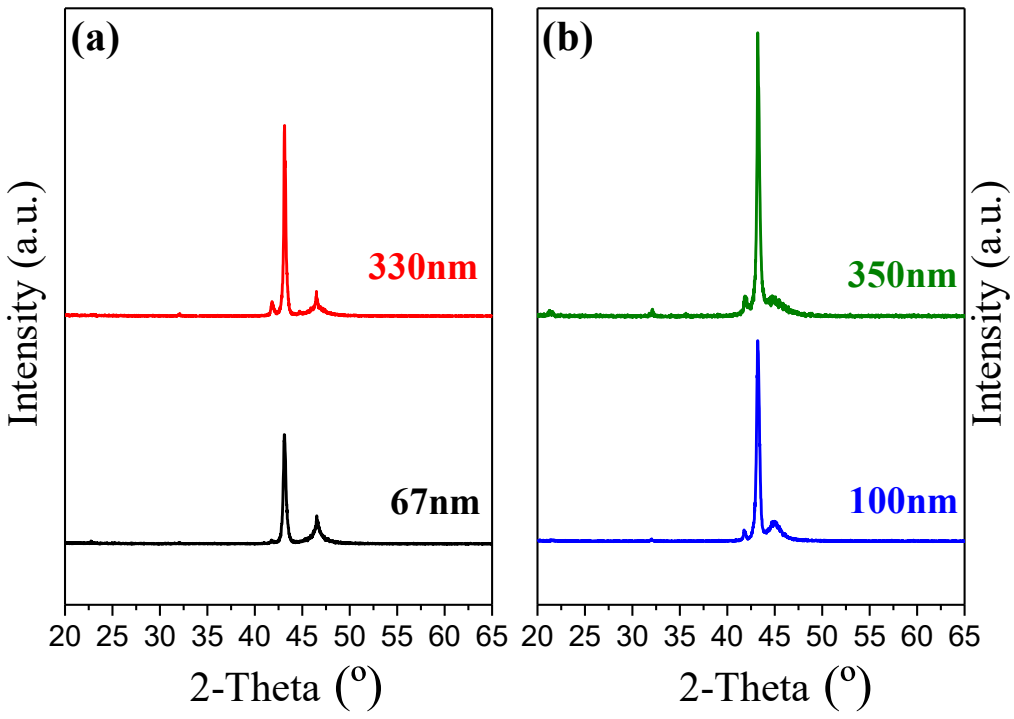

Figure 9. Thickness-dependent XRD diffraction patterns of magnetite films grown on $SrTiO_3$:Nb(001) (a) and $MgAl_2O_4$(001) (b).

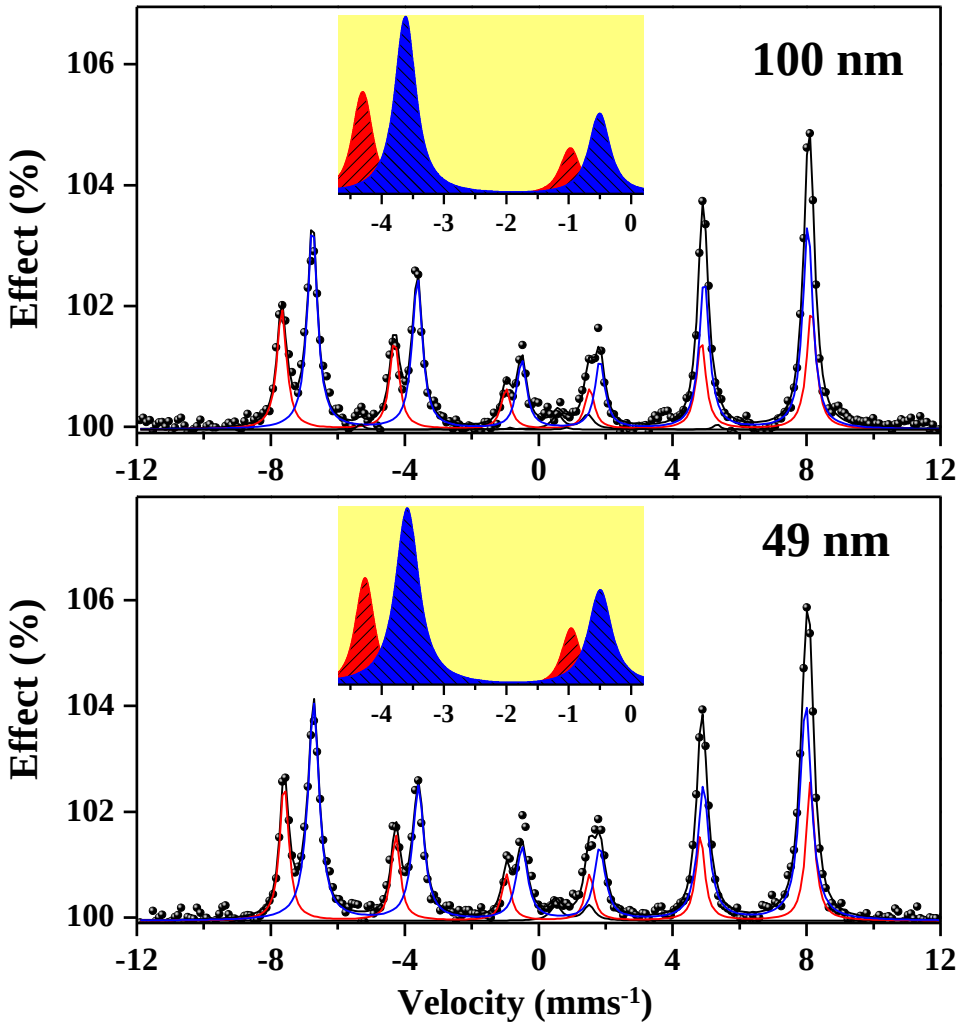

Figure 10. Thickness-dependent ICEMS spectra of epitaxial Fe_3O_4 films grown on MgO(001). The symbols are the experimental data acquired at RT for the thick (bottom graph) and the thin (bottom) film. Continuous black lines are the best fits with the two sextet components, as expected for magnetite. The corresponding resonances S_A and S_B are depicted with solid red and blue lines, respectively. $S_B/S_A = 1.9$ for the two films. The insets are zooms of the corresponding fits to visualize clearly that the area ratio x of the lines 2 and 3 of sextets is lower for the thinner film, suggesting that the magnetization of the thinner film is more out-of-plane.

spectra reflect high stoichiometric magnetite films and there is a non-negligible variation of T_V with both substrate and thickness. Figure 10 compares ICEMS spectra recorded from two magnetite films with different thickness deposited on MgO(001). The spectra were fitted with the same criteria and Mössbauer parameters described before (see Fig. 4). Similarly, the area ratio S_B/S_A found is 1.9 for both magnetite films, indicating that are of stoichiometric composition [44]. The x parameter, i.e., the area ratio of the lines 2 and 3, is 2.2 for the thicker film and 1.8 for the thinner one, as clearly show the corresponding insets of Fig. 10, indicating that the magnetization of the thinner film is

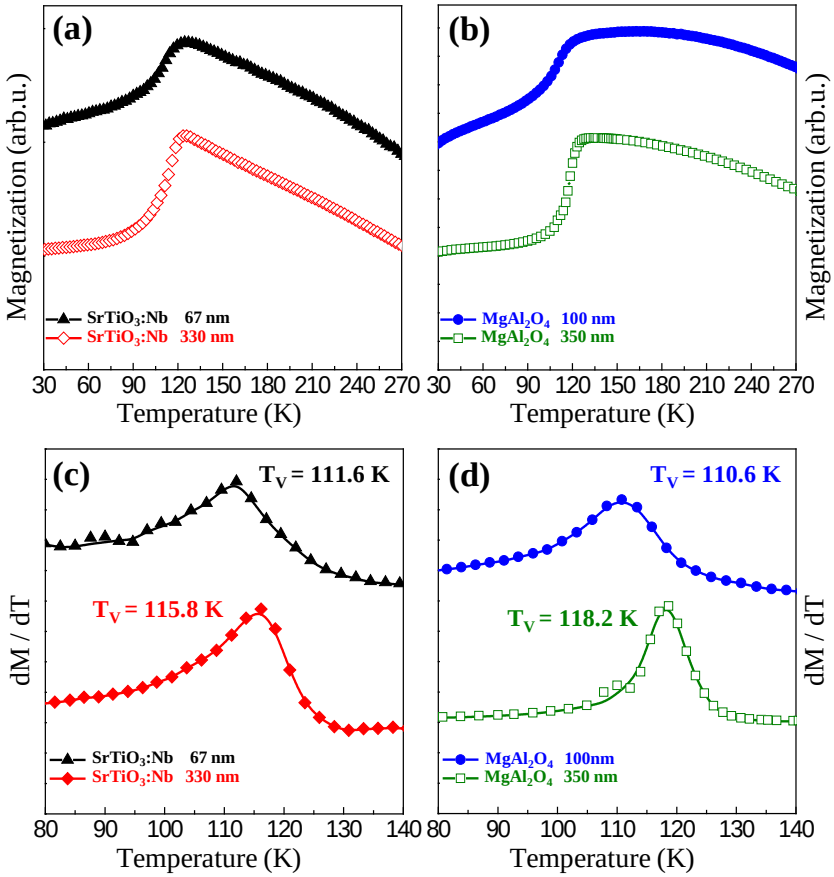

Figure 11. Thickness-dependent Verwey temperature transition (T_v) of films grown on $SrTiO_3$:Nb(001) (left graphs, a. and c.) and $MgAl_2O_4$(001) (right, b. and d.) substrates. In the top graphs are plotted the evolution of magnetization of the films during warming with an in-plane applied field of 2 kOe. On the bottom graphs are plotted the corresponding temperature evolution of dM/dT. For clarity, different colors and shapes have been used for the different Fe_3O_4 films. Note that T_v increases, getting closer to the bulk one, as thickness increases.

more out-of-plane than in the thicker one.

Each of the top graphs of Fig. 11 compares the magnetization evolution with temperature for different film thicknesses grown on different substrates. As it was previously mentioned, there is a reduction of the Verwey transition temperature to lower temperatures as the thickness decreases. Comparing the films grown on STO:Nb and MAO, the latter shows higher T_V values, i.e., closer to the bulk one, probably due to the smaller strain found on this film. As mentioned in the introduction, T_V is very sensitive to stoichiometry [8] but also to strain [55] and to the presence of structural defects [9, 24], even in highly stoichiometric films. Most work on epitaxial (compressive) films show a reduced T_V (we note that magnetite films prepared under tensile strain have recently shown substantially higher values than the bulk [55]). In turn, T_V decreases as the number of defects increases [46]. For example, magnetite films often present antiphase domain boundaries (APBs) [36, 46], as discussed later. APBs densities can be related

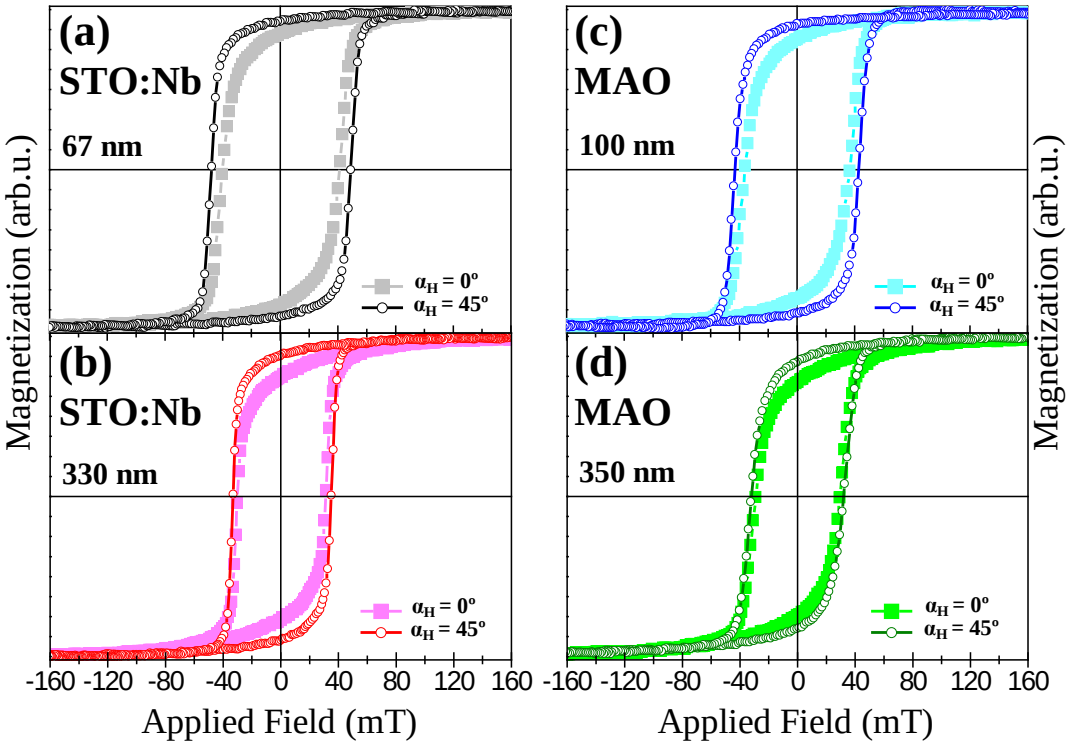

Figure 12. Selected in-plane hysteresis loops (easy and hard axis) comparing the influence of the thickness of epitaxial Fe_3O_4 films grown on STO:Nb(001) (left graphs) and MAO(001) (right). (a) 67 nm and (b) 330 nm deposited on $SrTiO_3$:Nb, and (c) 100 nm and (d) 350 nm deposited on $MgAl_2O_4$.

to the deposition temperature [46], and decreased by post-deposition annealing. So, for films with compressive strain grown on different substrates, the larger strain (films grown on STO:Nb), the lower T_V. In addition, thick films are at high temperature for longer times during fabrication, which should result in fewer defects and thus a larger T_V. The other observed dependenciy, i.e., of the out-of-plane magnetization component, will be analyzed when discussing the dependence of magnetic properties with the film thickness.

Representative hysteresis loops acquired at $\alpha_H = 0°$ and 45° comparing the magnetic behavior of Fe_3O_4 films with different thickness are displayed in Fig. 12. The left (right) graphs correspond to films grown on STO:Nb (MAO). The top (bottom) graphs compare loops of the thinner (thicker) films. All hysteresis show single loop behavior, and the thicker the film the smaller the coercivity and the remanence. In addition, the fourfold symmetry is clearly observed for all films grown on the (001)-oriented substrates, with the maxima of both coercivity and remanence lying along the ⟨100⟩ surface crystal directions, and the corresponding minima along the ⟨110⟩ directions. This magnetic symmetry is clearly observed in the polar plot representation of both coercivity and remanence shown in Fig. 13. Each polar-plot compares different thickness. The trend occurrs for the whole angular range. The coercivity and remanence

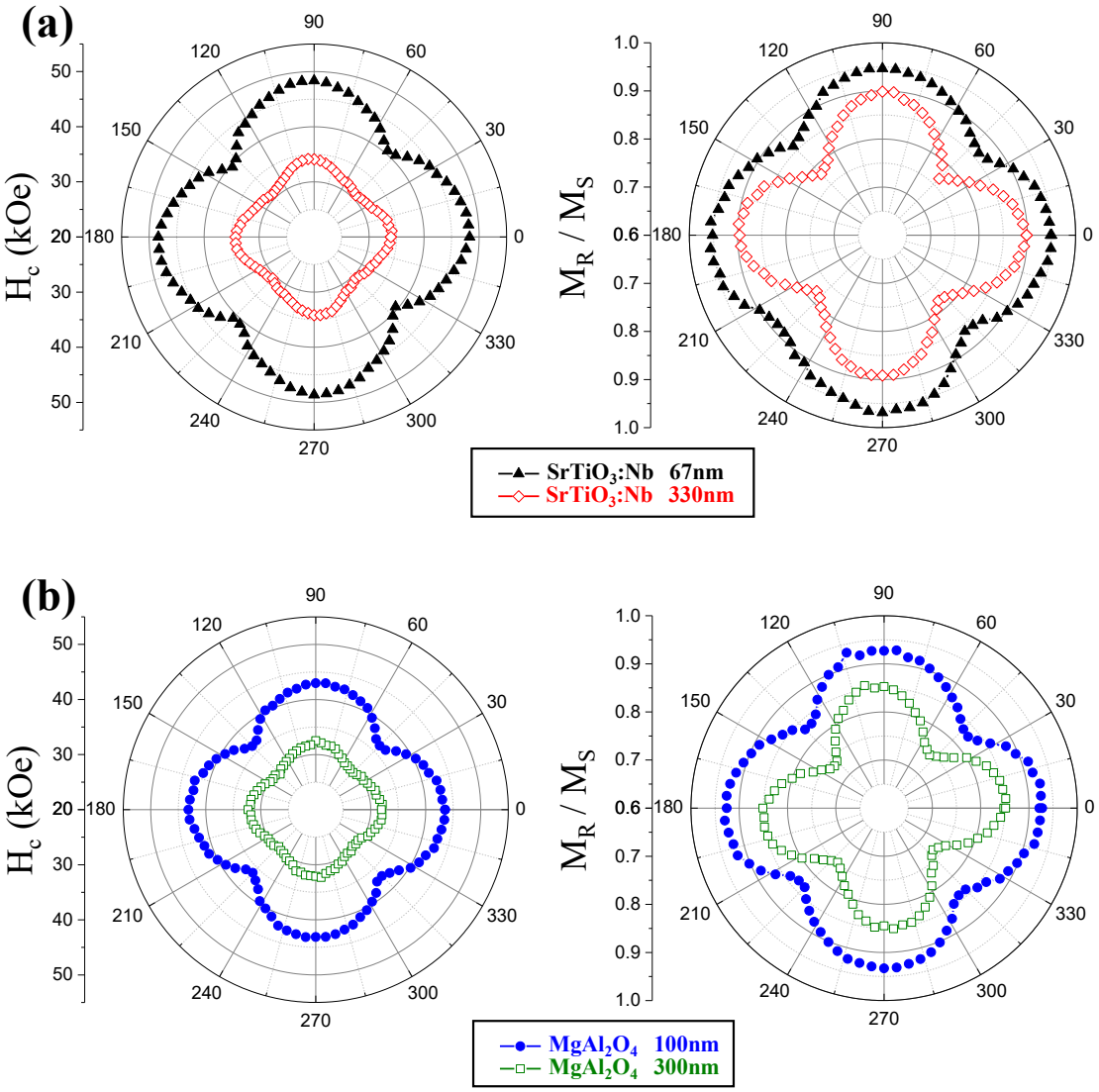

Figure 13. Angular evolution of in-plane H_C and M_R/M_S of Fe_3O_4 thin films deposited on $SrTiO_3$:Nb substrates with thickness of 67 nm (full triangles, black) and 330 nm (open diamonds, red), and $MgAl_2O_4$ substrates with thickness of 100 nm (full circles, blue) and 350 nm (open squares, green).

are smaller in the case of the thicker films. The fourfold magnetic symmetry is preserved for magnetite thicknesses as large as 450 nm.

The thickness-dependent coercivity along the easy direction for all films investigated has been plotted in Fig. 14. At a glance, the coercivity decreases as the film thickness increases, independently of the substrate used. A similar scenario but with smaller coercivity values is found for the other angular conditions. The coercivity follows an inverse law with the film thickness, whose accuracy is evident in the inset of the figure.

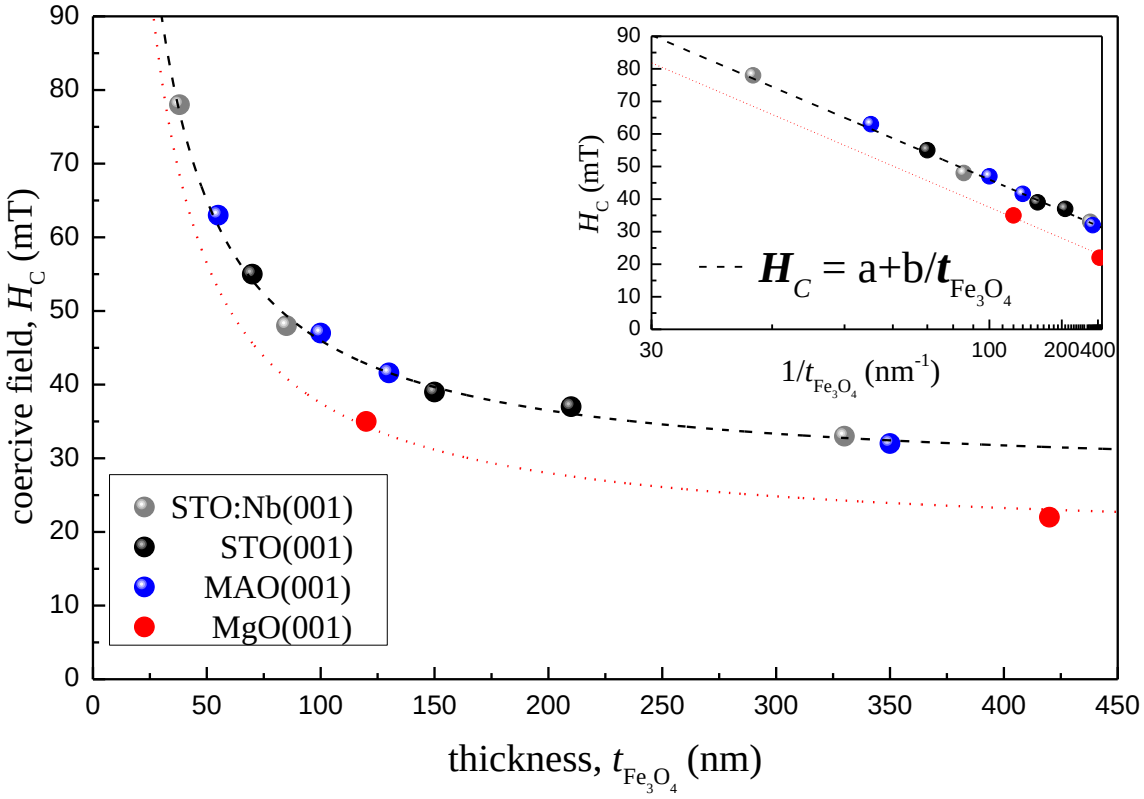

Figure 14. Thickness-dependent coercivity of epitaxial magnetite films. Inset: corresponding coercivity *vs.* 1/thickness plot. The experimental H_C values (symbols) have been derived from the hysteresis loops acquired with the field along the [100] direction, i.e., e.a., as those shown in Fig. 12. Different colors have been used for the films grown on different substrates. The dashed line is a fit to the coercivity using an inverse law with thickness, as discussed in the text.

4. Discussion

The substrate symmetry is related to the isotropic and anisotropic magnetic behavior found in the different films. Amorphous and hexagonal (non-cubic) substrate surfaces promote polycrystalline magnetite films and isotropic magnetic behavior, whereas (001)-oriented (cubic) substrate surfaces provide epitaxial (001)-oriented magnetite films with an effective fourfold (biaxial) magnetic anisotropy. In order to understand the rest of the observed features, i.e. the particular orientation of the easy axes, the changes in the out-of-plane magnetization or the evolution of the Verwey temperature and the changes in remanence and coercivity with temperature it is necessary to introduce the effects of the natural growth defects,(i.e., APBs), as well as thickness effects on (pinned) domain wall dynamics.

Thus we suggest that the magnetic features of IR-PLD grown pure magnetite films have three origins which are not independent of each other:

- Substrate-control of magnetic symmetry, resulting in the isotropic magnetic

behavior in the polycrystalline magnetite films and the fourfold magnetic anisotropy in the (001)-oriented epitaxial magnetite films.

- Antiphase boundaries (APBs)-control T_V and promote a magnetic symmetry along the $\langle 100 \rangle$ directions, i.e., rotated 45° with respect to the bulk projected directions.
- Dimensionality-control of coercive field, following an inverse law dependence with the film thickness.

We start by discussing the role of antiphase domain boundaries.

4.1. Antiphase Boundaries

Observations of high coercivities, high saturation fields, out-of-plane magnetization [36], superparamagnetism in ultrathin films [47], biaxial anisotropy induced by growth of magnetite films on MGO stepped substrates [48], as well as pinned magnetic domain structures [49] have all been attributed to antiphase domain boundaries (APBs) [36].

An antiphase domain boundary (APB) in a magnetite film appears when two islands of magnetite, separated by a non-integer multiple of the unit cell, coalesce. In such case, while the atomic lattice is continuous across the boundary, the cations order is disrupted. The presence of APBs in magnetite films has been extensively investigated in films grown on MgO(001) [13, 46], which have an almost perfect lattice mismatch but with different structures (spinel/cubic), and more recently on MAO (111) [50] which share the same structure (spinel/spinel) but have an small lattice mismatch (3%). In both cases, magnetite films show APBs. Moreover, it was found that the density of APBs is related to the deposition temperature, and can be decreased by post-deposition annealing. Under the same temperature growth conditions, the average domain size within the APB increases with the square root of the thickness, i.e., APBs density decreases following an inverse law with the square root of the thickness [13]. The increase in domain size and the decrease in the number of boundaries is a consequence of the APBs annealing out of the films with time at high temperature during growth and during annealing [46], as expected from diffusive antiphase boundary coarsening theory [51].

The effective magnetic easy axes found in the epitaxial films of this study, i.e., along the in-plane $\langle 100 \rangle$ directions, can be correlated with the directionality and the magnetic coupling of the APBs formed during growth [13]. APB shifts can be formed based on the different translation and rotation symmetry respectively for the case of the first Fe_3O_4 monolayer and the (001)-oriented surface. The influence of APBs on magnetic properties comes from the existence of specific geometries of the Fe-O-Fe arrangements not present in perfect bulk magnetite. The nature of magnetic coupling across APBs can be either antiferromagnetic or ferromagnetic, as recently show by atomic-resolution transmission electron microscopy and differential phase contrast imaging measurements [56]. For example, a given fraction of APBs comprises aligned Fe^{+3}-O-Fe^{+3} bonds (see Fig.1 of ref. [13]) which are known to create extremely strong antiferromagnetic superexchange interaction, resulting in a strong antiferromagnetic coupling along the $\langle 110 \rangle$ magnetite

surface directions. This might hinder the magnetic orientation along this direction, even in the case that it would correspond with the expected (bulk) anisotropy direction. In contrast, $\langle 100 \rangle$ APBs are expected to couple ferromagnetically. This might favor the magnetic orientation along $\langle 100 \rangle$ directions.

Further effects of these structural defects on the magnetic and transport properties of magnetite films are the high fields required to saturate the magnetization [36] and the large magnetoresistive effects [48]. The presence of APBs is the origin of rotation of the spins in the material and the formation of a complicated spin structure, due to the strong antiferromagnetic coupling at APBs and with a partial out-of-plane spin orientation around them, which depends on the external field [57]. Therefore, a smaller density of APBs will result in a decrease of the effective out-of-plane spin orientation.

The density and directionality of APBs have been analyzed extensively by Celotto and coworkers for different magnetite thicknesses and thermal treatments by using rose diagrams from image analysis on dark field images [13]. The density of APBs (domain size) decreases (increases) with film thickness and with increasing growth or annealing temperature. In turn, the directionality of the APBs is predominantly oriented close to $\pm\,[100]$ and $\pm\,[010]$ directions. This would make easier the magnetic orientation along this direction. Remarkably, the APBs directionality depicted in the rose diagrams of Fig.4 in ref. [13] closely resemble the polar-plots of magnetic properties discussed and presented previously (see Fig. 8 and Fig. 13).

We thus suggest that the epitaxial films (i.e., those grown on STO:Nb, STO, MAO, and MgO) present substantial densities of APBs oriented as reported in ref. [13]. Within this scenario, APBs may act as pinning centers making harder the magnetic orientation along specific directions, and making easier the most distant to the latter. In this sense, the effective hard axis directions lie along the $\langle 110 \rangle$ directions, from antiferromagnetic coupling between APBs, whereas the effective easy axes are aligned along the $\langle 100 \rangle$ directions.

The presence and inferred evolution of APBs explains the dependence of our ICEMS observations with thickness. All films investigated by ICEMS present an out-of-plane perpendicular component, which has not been detected by MOKE. This out-of-plane component is presumably originated from APBs in the films wiht a local antiferromagnetic ordering [57, 58], which have extremely high coercive fields [57] and are thus not detectable with our MOKE setup. This component is more prominent (lower x) for the thinner films (Fig. 10). So thinner films should have a somewhat higher APBs density. This is in line with the known behavior of APBs, which is reduced for samples annealed at high temperature: as all the films were grown at 750 K and at the same rate, the thicker films are kept at high temperature for longer times.

4.2. Reversal processes

Magnetization reversal is determined by the film microstructure (morphology, roughness, defects density), and by the magnetic properties including the anisotropy. The basic

magnetization processes in ferromagnetic systems are magnetization rotation, nucleation of inverted magnetic domains and motion of magnetic domains walls.

In the case of magnetic film with well defined magnetic anisotropies, coming from a saturated state and decreasing the applied field strength, the magnetization rotates in order to be aligned with the magnetization easy axis direction. At zero field the magnetization remanence depends on the angle between the direction of the last external field used and the anisotropy axis. From the remanent state, upon reversing the field orientation, the magnetization rotates until at an specific field a reversed magnetic domain nucleates, usually at a low coordination site. The reversal then continues by a further propagation of the magnetic domain wall, driven by the pressure exerted by the external field. Within this scenario, coercivity is a property related to the rate at which magnetic relaxation between the remanent and demagnetized states takes place. The relaxation process involves displacements of magnetic domain walls. For instance, APBs can act as pinning centers for the domain wall movement hardening the reversal.

Simple models based on the energy stored in a domain wall have been proposed in order to analyze the dependence of $H_{\rm C}$ with the thickness of a FM film $t_{\rm FM}$. This energy arises, among others, from exchange, anisotropy, and magnetostatic contributions, and depends on the type of wall under motion (i.e., Bloch or Neel type). In particular, while in both cases the models predict that the coercivity scales with the saturation magnetization, in the case of Neel wall motion the coercivity is proportional to $t_{\rm FM}$ whereas for Bloch wall motion it is inversely proportional to $t_{\rm FM}$. Neel walls are common in (ultrathin) films where the exchange length, c.a. few nm in FM, is very large compared to the thickness. For the case of our films, with thicknesses between 30 to 450 nm, Bloch type (bulk-like) domain walls must be considered. The inverse law with thickness predicted by the bulk-like model has been already proved experimentally in FM films [52, 53].

In the case of the films studied, apart from the weak expected evolution of the density of APB defects with the thickness inferred from ICESM, the rest of structural parameters are similar between each of the epitaxial films. In fact, all have well-defined fourfold-symmetric magnetic anisotropy (which is however rotated 45° from the projected bulk directions) and similar values of crystal grain size (40 to 60 nm), strain ($< 1\%$), and surface roughness (< 1 nm) on flat areas). Therefore the $1/t_{\rm Fe_3O_4}$ law found in these films, independently of the substrate used, can be explained by the general behaviour of thin layers with Bloch type domain walls, i.e., bulk-like layers, mediated by the APBs. This is also supported by the thickness dependence of the remanent magnetization. The thinnest samples show an M_R/M_S ratio close to 1, ratio which decreases as the thickness increases. The APB-induced unexpected magnetic anisotropy also diminishes, as the density of APBs is somewhat reduced with thickness.

Further proof that the origin of observed magnetic anisotropy in the (001)-oriented films is related to the morphological distribution of the APB defects is the fact that the associated phenomena is different from that usually found in epitaxial (001)-oriented cubic films. Fig. 15 compares representative vectorial-resolved measurements of the

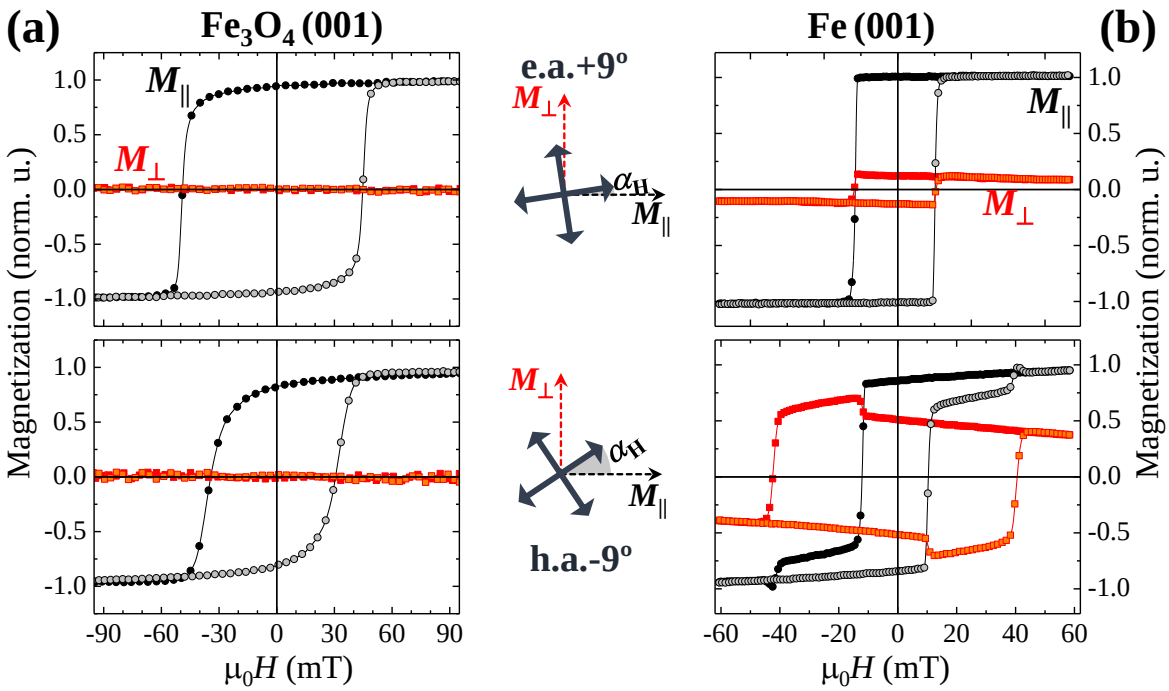

Figure 15. Selected vectorial-resolved hysteresis loops of films with fourfold magnetic symmetry acquired at indicated angles α_H: $Fe_3O_4(001)$ (a); Fe(001) (b). The corresponding measure geometries, where the e.a. directions (magnetization components) are indicated by thick continuous (thin dashed) arrows are shown in the middle. The $M_{\parallel}(H)$ and $M_{\perp}(H)$ loops are represented by circles and squares, respectively. The two branches have been depicted with different filled symbols to clarify the evolution of the magnetization.

epitaxial films (left graphs) with the ones of a cubic Fe(001) film (right) acquired with the field oriented nearby the characteristic easy (top) and hard (bottom) directions. In general, both systems present fourfold symmetry, i.e., the magnetic properties are repeated every 90°, but the reversal pathways are quite different. For example, for the Fe(100) film, the reversal is characterized by a strong angular dependence in the number of irreversible transitions [42]. In particular, when the field orientation is closed to the easy directions, an irreversible transition (corresponding to nucleation and propagation of 180-oriented domain walls) is observed, whereas two irreversible transitions (related to nucleation and propagation of 90-oriented domain walls) are found close to the hard directions. Note that this is also easier to identify in the $M_{\perp}(H)$ loop. In clear contrast, the vectorial-resolved loops of any of the epitaxial magnetite films investigated show just one irreversible transition and only in the $M_{\parallel}(H)$ loop, being almost negligible the $M_{\perp}(H)$ loop. The latter could be explained by opposite magnetization rotation pathways, i.e., above and below the field direction, taking place before and after the sharp transition. This would cancel out the $M_{\perp}$ signal at any field, i.e., $M_{\perp}(H) \approx 0$, as observed experimentally.

5. Conclusions

High quality stoichiometric magnetite (Fe_3O_4) films grown by infrared pulsed laser deposition (IR-PLD) on different substrates (i.e., $SrTiO_3(001)$, $MgAl_2O_4(001)$, $MgO(001)$, $Al_2O_3(0001)$ and amorphous Si/SiO_2) have been investigated in order to study the influence of the substrate, orientation, and thickness on their magnetic behavior.

All films consist of nanocrystalline stoichiometric magnetite with very small strain ($< 1\%$) and a Verwey transition (T_V) between 110-120 K, i.e., close to the transition temperature of bulk magnetite (125 K). T_V depends on microstructure and thickness, increasing as the thickness increases. Room temperature angular-dependent measurements reveal isotropic behavior for magnetite films grown on $Al_2O_3(0001)$ and Si/SiO_2, whereas an in-plane fourfold symmetry magnetic behavior for all films grown on (001)-oriented surfaces, and with the easy axes lying along the Fe_3O_4 [010] and [100] directions, i.e., rotated with respect to the bulk projected directions. Remarkably, the fourfold magnetic symmetry is shown even in 400 nm thick films. In turns, the coercive field (H_C) depends on microstructure and film thickness. The largest (lowest) H_C value has been found for the thinner film grown on a single crystal $SrTiO_3(001)$ (amorphous Si/SiO_2) surface. Moreover, the coercivity follows an inverse law with film thickness, as predicted with a simple bulk-like model.

These results demonstrate that it is possible to artificially control the magnetic behavior of stoichiometric IR-PLD grown Fe_3O_4 films by exploiting substrate-induced anisotropy and thickness-controlled coercivity, helping paving the way to incorporate magnetite in future magnetic-based applications.

6. Acknowledgements

This research was supported by the Regional Government of Madrid through Projects S2013/MIT-2850 (NANOFRONTMAG) and P2018/NMT-4321 (NANOMAGCOST) and by the Spanish Ministry of Economy and Competitiveness (MINECO) through Projects FIS2016-78591-C3-1-R, CTQ2016-75880-P, and MAT2017-89960-R. M. O. thanks CSIC for contract and E.R. thanks MINECO for the tenure of a Ramón y Cajal contract (No. RYC-2011-08069). IMDEA Nanoscience is supported by the 'Severo Ochoa' Programme for Centres of Excellence in R&D, MINECO [grant number SEV-2016-0686].

References

[1] Mills A A, 2004, The lodestone: History, physics, and formation, *Ann. Sci.*, **61** 273319

[2] Van Der Zaag P, Bloemen P, Gaines J, Wolf R, Van Der Heijden P, Van de Veerdonk R and De Jonge W, 2000, On the construction of an Fe_3O_4-based all-oxide spin valve, *J. Magn. Magn. Mater.*, **211** 301308

[3] Ziese M, 2002, Extrinsic magnetotransport phenomena in ferromagnetic oxides, *Rep. Prog. Phys.*, **65** 143

[4] Wada E, Watanabe K, Shirahata Y, Itoh M, Yamaguchi M and Taniyama T, 2010, Efficient spin injection into GaAs quantum well across Fe_3O_4 spin filter, *Appl. Phys. Lett.*, **96** 102510

[5] Fonin M, Dedkov Y S, Pentcheva R, Rüdiger U and Güntherodt G, 2007, Magnetite: a search for the half-metallic state, *J. Phys-Cond. Mat.*, **19** 315217

[6] Walz F, 2002, The verwey transition; a topical review, *J. Phys-Cond. Mat.* **14** R285

[7] García J and Subías G, 2004, The verwey transition; a new perspective, *J. Phys-Cond. Mat.* **16** R145

[8] Aragón R, Buttrey D J, Shepherd J P and Honig J M, 1985, Influence of nonstoichiometry on the Verwey transition, *Phys. Rev. B* **31** 430

[9] Liu X, Rata A, Chang C, Komarek A and Tjeng L, 2014, Verwey transition in Fe_3O_4 thin films: Influence of oxygen stoichiometry and substrate-induced microstructure, *Phys. Rev. B*, **90** 125142

[10] Margulies, D. T., Parker, F. T., Spada, F. E., Goldman, R. S., Li, J., Sinclair, R., and Berkowitz, A. E., 1996. Anomalous moment and anisotropy behavior in Fe_3O_4 films. *Phys. Rev. B*, **53**(14), 9175.

[11] Van der Heijden P, Van Opstal M, Swüste C, Bloemen P, Gaines J and De Jonge W, 1998, A ferromagnetic resonance study on ultra-thin Fe_3O_4 layers grown on (001) MgO, *J. Magn. Magn. Mater.*, **182** 71-80

[12] Voogt, F. C., Fujii, T., Smulders, P. J. M., Niesen, L., James, M. A., and Hibma, T. (1999). NO_2-assisted molecular-beam epitaxy of Fe_3O_4, $Fe_3O_4 - \delta$, and γ- Fe_2O_3 thin films on MgO (100). *Phys. Rev. B*, **60**(15), 11193.

[13] Celotto S, Eerenstein W and Hibma T, 2003, Characterization of anti-phase boundaries in epitaxial magnetite films, *Eur. Phys. J. B* **36** 271-279.

[14] Moussy J B, 2013, From epitaxial growth of ferrite thin films to spin-polarized tunnelling, *J. Phys. D Appl. Phys.* **46** 143001

[15] Schemme T, Pathé N, Niu G, Bertram F, Kuschel T, Kuepper K and Wollschläger J, 2014, Magnetic anisotropy related to strain and thickness of ultrathin iron oxide films on MgO(001), *Mater. Res. Express.*, **2** 016101

[16] Yanagihara H, Myoka M, Isaka D, Niizeki T, Mibu K and Kita E, 2013, Selective growth of Fe_3O_4 and γ-Fe_2O_3 films with reactive magnetron sputtering, *J. Phys. D Appl. Phys.*, **46** 175004

[17] Prieto P, Prieto J E, Gargallo-Caballero R, Marco J F and de la Figuera J, 2015, Role of the substrate on the magnetic anisotropy of magnetite thin films grown by ion-assisted deposition, *Appl. Surf. Sci.*, **359** 742748

[18] Xiang H, Shi F, Rzchowski M S, Voyles P M and Chang Y A, 2010, Epitaxial growth and magnetic properties of Fe_3O_4 films on TiN buffered Si(001), Si(110), and Si(111) substrates *Appl. Phys. Lett.*, **97** 092508

[19] Prieto P, de la Figuera J, Mart ín-Garc ía L, Prieto J E and Marco J F, 2016, Fourfold in-plane magnetic anisotropy of magnetite thin films grown on tin buffered Si(001) by ion-assisted sputtering, *J. Mater. Chem. C*, **4** 7632-7639

[20] Arenholz E, van der Laan G, Chopdekar R V and Suzuki Y, 2006, Anisotropic X-ray magnetic linear dichroism at the Fe $L_{2,3}$ edges in Fe_3O_4, *Phys. Rev. B*, **74** 094407

[21] Hamie A, Dumont Y, Popova E, Fouchet A, Warot-Fonrose B, Gatel C, Chikoidze E, Scola J, Berini B and Keller N, 2012, Investigation of high quality magnetite thin films grown on $SrTiO_3$ (001) substrates by pulsed laser deposition, *Thin Solid Films*, **525** 115120

[22] Sanz M, Oujja M, Rebollar E, Marco J F, de la Figuera J, Monti M, Bollero A, Camarero J, Pedrosa F J, García-Hernández M et al, 2013, Stoichiometric magnetite grown by infrared nanosecond pulsed laser deposition, *Appl. Surf. Sci.*, **282** 642651

[23] Monti M, Sanz M, Oujja M, Rebollar E, Castillejo M, Pedrosa F J, Bollero A, Camarero J, Cunado J L F, Nemes N M et al, 2013, Room temperature in-plane $\langle 100 \rangle$ magnetic easy axis for $Fe_3O_4/SrTiO_3$ (001): Nb grown by infrared pulsed laser deposition, *J. Appl. Phys.*, **114** 223902

[24] Dho J, Kim B and Ki S, 2016, Substrate Effects on In-Plane Magnetic Anisotropy and Verwey

Transition Temperatures of (100) Magnetite (Fe_3O_4) Films, *IEEE T. Magn.*, **52** 14

[25] de la Figuera J, Vergara L, NDiaye A T, Quesada A and Schmid A K, 2013, Micromagnetism in (001) magnetite by spin-polarized low-energy electron microscopy, *Ultramicroscopy*, **130** 77-81

[26] Horng L, Chern G, Chen M, Kang P and Lee D, 2004, Magnetic anisotropic properties in Fe_3O_4 and $CoFe_2O_4$ ferrite epitaxy thin films, *J. Magn. Magn. Mater.*, **270** 389396

[27] Nagahama T, Matsuda Y, Tate K, Kawai T, Takahashi N, Hiratani S, Watanabe Y, Yanase T and Shimada T, 2014, Magnetic properties of epitaxial Fe_3O_4 films with various crystal orientations and tunnel magnetoresistance effect at room temperature, *Appl. Phys. Lett.*, **105** 102410

[28] Chichvarina O, Herng T, Xiao W, Hong X and Ding J, 2015, Magnetic anisotropy modulation of epitaxial Fe_3O_4 films on MgO substrates, *J. Appl. Phys.*, **117** 17D722

[29] Dho J, Kim B g and Ki S, 2015, Distinctive uniaxial magnetic anisotropy and positive magnetoresistance in (110)-oriented Fe_3O_4 films, *J. Appl. Phys.*, **117** 163904

[30] Cheng J, Sterbinsky G and Wessels B, 2008, Magnetic and magneto-optical properties of heteroepitaxial magnetite thin films, *J. Cryst. Growth.*, **310** 3730-3734

[31] Kale S, Bhagat S, Lofland S, Scabarozi T, Ogale S, Orozco A, Shinde S, Venkatesan T, Hannoyer B, Mercey B et al.,2001, Film thickness and temperature dependence of the magnetic properties of pulsed-laser-deposited Fe_3O_4 films on different substrates, *Phys. Rev. B*, **64** 205413

[32] Hassan S S, Xu Y, Wu J and Thompson S M, 2009, Epitaxial growth and magnetic properties of half-metallic Fe_3O_4 on Si(100) using MgO buffer layer, *IEEE T. Magn.*, **45** 4357-4359

[33] Zhang W, Zhang J, Wong P, Huang Z, Sun L, Liao J, Zhai Y, Xu Y and van der Laan G, 2011, In-plane uniaxial magnetic anisotropy in epitaxial Fe_3O_4-based hybrid structures on GaAs(100), *Phys. Rev. B*, **84** 104451

[34] Huang Z, Hu X, Xu Y, Zhai Y, Xu Y, Wu J and Zhai H, 2012, Magnetic properties of ultrathin single crystal Fe_3O_4 film on InAs (100) by ferromagnetic resonance, *J. Appl. Phys.*, **111** 07C108

[35] Cuñado J L F, Bollero A, P érez-Castañeda T, Perna P, Ajejas F, Pedrosa J, Gud ín A, Maldonado A, Niño M A, Guerrero R et al., 2017, Emergence of the Stoner-Wohlfarth astroid in thin films at dynamic regime, *Sci. Rep.*,**7** 13474

[36] Margulies D, Parker F, Rudee M, Spada F, Chapman J, Aitchison P and Berkowitz A, 1997, Origin of the anomalous magnetic behavior in single crystal Fe_3O_4 films, *Phys. Rev. Lett.*, **79** 5162

[37] Eerenstein W, Palstra T, Saxena S and Hibma T, 2002, Spin-polarized transport across sharp antiferromagnetic boundaries, *Phys. Rev. Lett.*, **88** 247204

[38] Ashfold M N, Claeyssens F, Fuge G M and Henley S J, 2004, Pulsed laser ablation and deposition of thin films, *Chem. Soc. Rev.*, **33** 23-31

[39] Bollero A, Ziese M, Höhne R, Semmelhack H, Köhler U, Setzer A and Esquinazi P, 2005, Influence of thickness on microstructural and magnetic properties in Fe_3O_4 thin films produced by PLD, *J. Magn. Magn. Mater.*, **285** 279-289

[40] Momma, K and Izumi, F., 2011, VESTA 3 for Three-Dimensional Visualization of Crystal, Volumetric and Morphology Data, *J. Appl. Crystallogr.* 44, 1272.

[41] J.R. Gancedo, J. R., Gracia, M., and Marco, J.F., 1991. CEMS methodology. *Hyperfine Interactions* **66**, 83-93.

[42] Jiménez E, Mikuszeit N, Cuñado J, Perna P, Pedrosa J, Maccariello D, Rodrigo C, Niño M, Bollero A, Camarero J et al., 2014, Vectorial Kerr magnetometer for simultaneous and quantitative measurements of the in-plane magnetization components, *Rev. Sci. Instrum.*, **85** 053904

[43] Cuñado J L F, Pedrosa J, Ajejas F, Bollero A, Perna P, Terán F J, Miranda R and Camarero J, 2015, Note: Vectorial-magneto optical Kerr effect technique combined with variable temperature and full angular range all in a single setup, *Rev. Sci. Instrum.*, **86** 046109

[44] Vandenberghe R, Barrero C, Da Costa G, Van San E and De Grave E, 2000, Mossbauer characterization of iron oxides and (oxy) hydroxides: the present state of the art, *Hyperfine Interact.*, **126** 247-259

[45] Liu X, Rata A, Chang C, Komarek A and Tjeng L, 2014, Verwey transition in Fe_3O_4 thin films: Influence of oxygen stoichiometry and substrate-induced microstructure, *Phys. Rev. B*,

90 125142

[46] Eerenstein W, Palstra T, Hibma T and Celotto S, 2003, Diffusive motion of antiphase domain boundaries in Fe_3O_4 films, *Phys. Rev. B*, **68** 014428

[47] Voogt F, Palstra T, Niesen L, Rogojanu O, James M and Hibma T, 1998, Superparamagnetic behavior of structural domains in epitaxial ultrathin magnetite films, *Phys. Rev. B*, **57** R8107

[48] McGuigan L, Barklie R, Sofin R, Arora S and Shvets I, 2008, In-plane magnetic anisotropies in Fe_3O_4 films on vicinal MgO (100), *Phys. Rev. B*, **77** 174424

[49] Wei J, Knittel I, Hartmann U, Zhou Y, Murphy S, Shvets I and Parker F, 2006, Influence of the antiphase domain distribution on the magnetic structure of magnetite thin films, *Appl. Phys. Lett.*, **89** 122517

[50] McKenna K P, Hofer F, Gilks D, Lazarov V K, Chen C, Wang Z and Ikuhara Y, 2014, Atomic-scale structure and properties of highly stable antiphase boundary defects in Fe_3O_4, *Nat. Commun.*, **5**

[51] Allen S M and Cahn J W, 1979, A microscopic theory for antiphase boundary motion and its application to antiphase domain coarsening, *Acta. Metall. Mater.*, **27** 1085-1095

[52] Min H G, Kim S H, Li M, Wedding J and Wang G C, 1998, Thickness-dependent coercivity of ultrathin Co films on a rough substrate: Cu-buffered Si (111), *Surf. Sci.*, **400** 1928

[53] Camarero J, De Miguel J, Miranda R and Hernando A, 2000, Thickness-dependent coercivity of ultrathin Co films grown on Cu (111), *J. Phys-Cond. Mat.*, **12** 7713

[54] Bruns, D and Lindemann, SR and Kuepper, K and Schemme, T and Wollschläger, J, 2013, Fe_3O_4 films on Ag(001)-Generation of high-quality epitaxial ferrimagnetic metal oxide films, *Appl. Phys. Lett.*, **103** 052401

[55] Liu, XH, Chun-Fu C, Rata AD, Komarek AC, and Tjeng LH, 2016, Fe_3O_4 thin films: controlling and manipulating an elusive quantum material, *npj Quantum Materials* **1**, 16027.

[56] Chen, C., Li, H., Seki, T., Yin, D., Sanchez-Santolino, G., Inoue, K., Shibata, N., and Ikuhara, Y., 2018, Direct determination of atomic structure and magnetic coupling of magnetite twin boundaries. *ACS nano*, **12**(3), 2662-2668.

[57] Kalev, L. A., and Niesen, L., 2003, Nuclear resonance scattering study on the spin orientation in an epitaxial layer of Fe 3 O 4 on MgO (100). *Phys. Rev. B*, **67**(22), 224403.

[58] de la Figuera, J., and Marco, J.F., 2019, Magnetite and the Verwey transition, from gamma-rays to low-energy electrons, *Hyperfine Interactions*, DOI:10.1007/s10751-019-1577-8